CHEMISTRY OF MATERIALS

Article

pubs.acs.org/cm

Chemical Vapor Deposition of Carbon Nanotubes on Monolayer Graphene Substrates: Reduced Etching via Suppressed Catalytic Hydrogenation Using C_2H_4

Kitu Kumar, Youn-Su Kim, Xin Li, Junjun Ding, Frank T. Fisher, and Eui-Hyeok Yang*

Department of Mechanical Engineering, Stevens Institute of Technology, Castle Point-on-Hudson, Hoboken, New Jersey 07030, United States

Supporting Information

ABSTRACT: In most envisioned applications, the full utilization of a graphene-carbon nanotube (CNT) construct requires maintaining the integrity of the graphene layer during the CNT growth step. In this work, we exhibit an approach toward controlled CNT growth atop graphene substrates where the reaction equilibrium between the source hydrocarbon decomposition and carbon saturation into and precipitation from the catalyst nanoparticles shifts toward CNT growth rather than graphene consumption. By utilizing C_2H_4 feedstock, we demonstrate that the low-temperature growth permissible with this gas suppresses undesirable catalytic hydrogenation and dramatically reduces the etching of the graphene layer to exhibit graphene-CNT hybrids with continuous, undamaged structures.

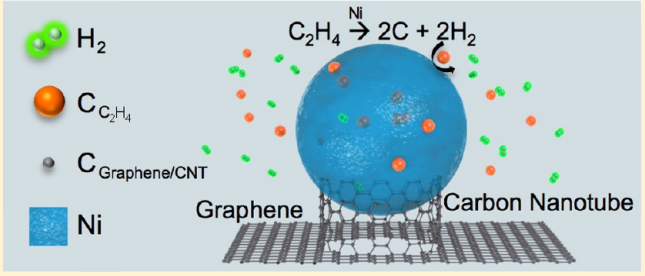

KEYWORDS: *graphene, carbon nanotube growth, catalytic hydrogenation, 3D nanoarchitectures, chemical vapor deposition*

INTRODUCTION

Recent efforts in fabricating 3D composite nanostructures consisting of 2D graphene and 1D nanomaterials of carbon[1−3] and conducting polymers[4] are of interest for a number of applications, including next-generation, high-capacity, fast-discharge supercapacitors. For these types of energy storage applications, the advantages of graphene, such as its large surface area-to-volume ratio and excellent conductivity, may be compromised because of self-aggregation, resulting in poor charge transfer among the graphene flakes, the 1D materials, and the current collector. The growth of 1D nanostructures such as carbon nanofibers[5,6] or nanotubes[7,8] directly on graphene[9] to yield hybrid 3D nanoarchitectures would, by design, circumvent this self-aggregation while maintaining low contact resistance to enable effective electron transfer.[7−10] In our previous work, CNTs were grown by chemical vapor deposition (CVD) directly on graphene using CH_4 gas as a carbon source, and the performance of the resulting 3D nanoarchitecture as an advanced electrical double-layer capacitor was characterized.[10] However, during this growth, the graphene layer was often found to be etched away at so-called "etched pits". The formation of these pits proceeded from hydrogenation[11−13] at 800 °C in the presence of nickel (Ni) catalyst nanoparticles ($(Ni)_{nanoparticle} + C_{graphene} + 2H_2 \rightarrow Ni + CH_4$).[14] Elongated etched lines in the graphene are attributed to etching by mobile nanoparticles. Subsequently, the addition of H_2 from the catalytic decomposition of the carbon source during the CNT growth step further contributes to the etching effect and can fully remove the graphene substrate. This etching process of the graphene substrate during CNT growth has thus far not been studied in the literature.

Here we show that the high hydrocarbon conversion rate of C_2H_4, at lower temperature than CH_4[16] used in our previous study,[10] allows for an approach to CNT growth atop graphene substrates through fine-tuning the process parameters including growth temperature and seed density. We confirm that the controlled use of C_2H_4 is essential for balancing the competing processes of carbon deposition and carbon removal, which ultimately block undesired etching of the graphene substrate during the CNT growth process.

RESULTS AND DISCUSSION

After graphene-CNT structures were fabricated (Scheme 1), scanning electron microscopy (SEM), Raman spectroscopy, and transmission electron microscopy (TEM) imaging were conducted to characterize the structure of the CNTs grown on graphene. Of fundamental importance was confirming the growth of (1) graphene on the substrate and (2) CNTs on the graphene. TEM images of graphene, the graphene-CNT interface, and CNTs were analyzed (Figure 1) to assess the quality of the grown samples. Graphene was found to be monolayer in the majority of regions, as characterized by AFM step height measurements[17] and further TEM imaging of the graphene lattice (Figure S1). Multiwalled CNTs were found to

Received: June 25, 2013
Revised: August 30, 2013
Published: September 2, 2013

Scheme 1. CNT Growth Process on a Graphene Substrate[a]

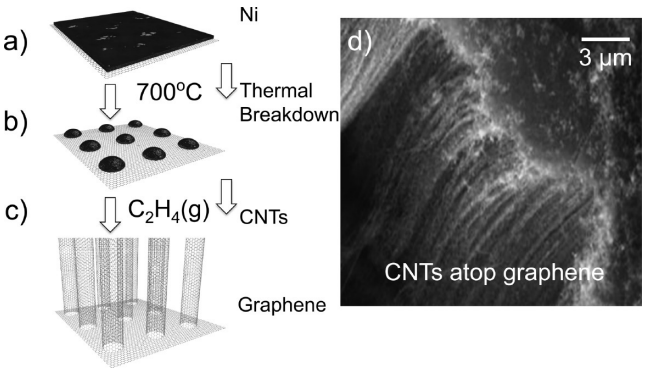

[a](a) Graphene with 3 nm of an electron beam-deposited Ni film. (b) Thermal treatment of the 3 nm Ni film to form Ni nanoparticles. (c) CNT growth from Ni catalyst nanoparticles. (d) SEM image of vertically grown CNTs atop a graphene substrate. The sample is intentionally broken and peeled off for the purpose of observation.

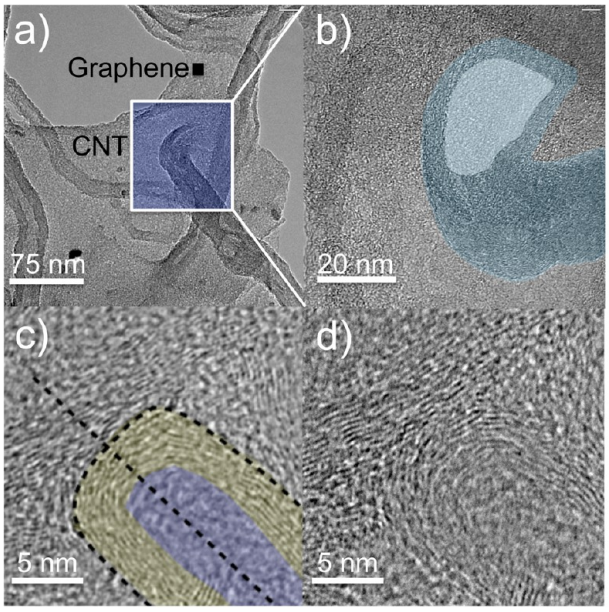

Figure 1. TEM images of the graphene-CNT hybrid. (a) Low-magnification TEM image of multiwalled CNTs growing out of the underlying graphene. The blue region highlights the root of the CNT originating from graphene. The average diameter for this CNT is 26.8 ± 1.9 nm. (b) Magnified, false-colored image of the highlighted region in panel a. The blue color indicates the CNT walls extending from the graphene support, and the white color further highlights the root region. (c) High-magnification, false-colored TEM image of a different CNT atop graphene. The yellow and purple colors highlight the CNT walls and hollow inner tube, respectively. The graphene planes within the yellow region are parallel to the tube growth axis (black dashed trace), verifying that CNTs have been grown.[15] The inner and outer tube diameters are 5.8 and 12.5 nm, respectively. (d) Unmarked image of the CNT in panel c.

have a root in the graphene lattice, as evidenced by Figure 1a. Figure 1b shows a CNT clearly growing out of the graphene layer. The ohmic contact between CNT and graphene, formed during such a growth,[18] is a necessity to facilitate charge transfer[19] between the two materials for energy storage applications.[10] Additionally, the graphene planes of the multiwalled CNTs run parallel to the growth axis of the tube, as shown in Figure 1c, confirming that CNTs, as opposed to carbon nanofibers, were grown in this process. For comparison, TEM images of a carbon nanofiber show a characteristic fishbone arrangement, as shown in Figure S2.

Raman spectra were taken at an excitation wavelength of 532 nm to assess the crystalline quality of the graphene-CNT structure. As shown in Figure 2a, the original as-grown

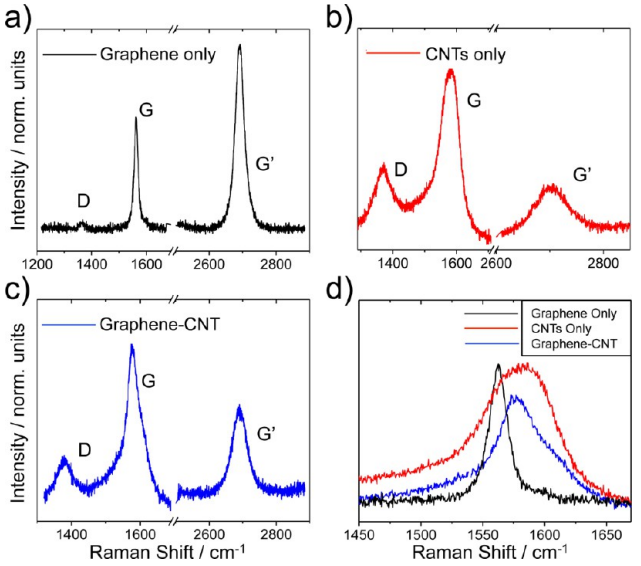

Figure 2. Raman spectra of (a) CVD-grown graphene, (b) CVD-grown multiwalled CNTs only, and (c) the graphene-CNT hybrid structure on SiO_2/Si substrate. (d) Magnification of the G bands of all three samples. Although the G band of graphene is sharp and symmetric, it is broad and asymmetric in the CNTs only and graphene-CNT sample because of a smeared splitting effect from the G^+ and G^- components.

graphene films exhibit the three distinctive peaks of sp^2 carbon, namely, D, G, and G′, corresponding to defects, E_{2g} vibrations of the sp^2 bonds, and a second-order double-resonance process distinctive in graphene, respectively.[20]

The G′ band peak of the graphene shows a higher peak intensity than the G band, with an intensity ratio, $I_{G'}/I_G$, of 1.57, and can be fitted to a sharp, symmetric Lorentzian with a full-width at half-maximum (fwhm) of 32 cm^{-1}. The D band at ∼1380 cm^{-1} is minimal, with an intensity ratio I_D/I_G ∼ 0.11, which is attributed to the presence of grain boundaries.[21] These characteristics strongly suggest that the grown graphene is high quality and monolayer.[22] In comparison, the Raman spectrum of CNTs only, presented in Figure 2b, features a broader, asymmetric, intense G-band peak with a fwhm of 40 cm^{-1}, a suppressed G′ band ($I_{G'}/I_G$ ∼0.4), and a broad D band. The Raman spectrum of CNTs grown on the graphene from Figure 2a presents similar characteristics (Figure 2c): a broad, asymmetric, intense G band, a G′ band that is less suppressed ($I_{G'}/I_G$ ∼0.7) than in the CNT case because of the presence of graphene, and a broad D band arising from the addition of the grown CNTs. The asymmetry that arises in the G bands of both CNTs only and the graphene-CNT hybrid (Figure 2d), compared to graphene only, is due to the splitting of the band into two components, G^- (∼1570 cm^{-1}) and G^+ (∼1610 cm^{-1}).[23] The G^- component arises from vibrations along the circumferential direction of the CNTs, whereas the G^+ component arises from vibrations along the tube growth axis.[24] This splitting is not pronounced because of a smearing

dx.doi.org/10.1021/cm402052z | Chem. Mater. 2013, 25, 3874−3879

effect from the presence of multiple diameter graphene walls in the CNT, but it contributes to the skew of each band. No radial breathing mode was observed in the graphene-CNT sample because of the smearing effect.[25] These results, along with the TEM characterization in Figure 1 and the AFM/TEM characterization in Figure S1, confirm the successful growth of monolayer graphene followed by the growth of CNTs on the graphene substrate.

To study the impact of the processing conditions on graphene etching during CVD, we first analyzed the impact of temperature during catalyst nanoparticle generation. In Figure 3a, a 3 nm Ni film atop graphene was exposed to Ar/H_2 (400/50 sccm) flow at 800 °C. This high-temperature process dewetted[26−28] the Ni film, forming catalyst nanoparticles with highly variant size (Figure 3c) and low density. Under this condition, which was intentionally created to detail the graphene etching phenomena, etched pits (Figure 3a, yellow dashed circles) appeared in graphene around the nanoparticles. Catalytic hydrogenation occurs at this temperature, wherein the carbon atoms in graphene enter the molten Ni droplet and subsequently react with H_2 at the surface of the droplet, forming CH_4 gaseous species.[11,29] The two principal particle sizes observed in Figure 3a,c are attributed to a surface-diffusion-based Ostwald ripening process.[30,31] The presence of certain etched lines (Figure 3a, white dashed lines) appear to be caused by etching from mobile nanoparticles, which continues until the energetics for the motion reaction cease. These etched pits and lines are capable of originating at this temperature at any high-energy, defectives sites in graphene such as grain boundaries. Indeed, the initiation of nanoparticle motion has been shown to occur due to attractive forces between the particle and carbon atoms with dangling bond, rather than with carbon atoms in the basal plane.[32]

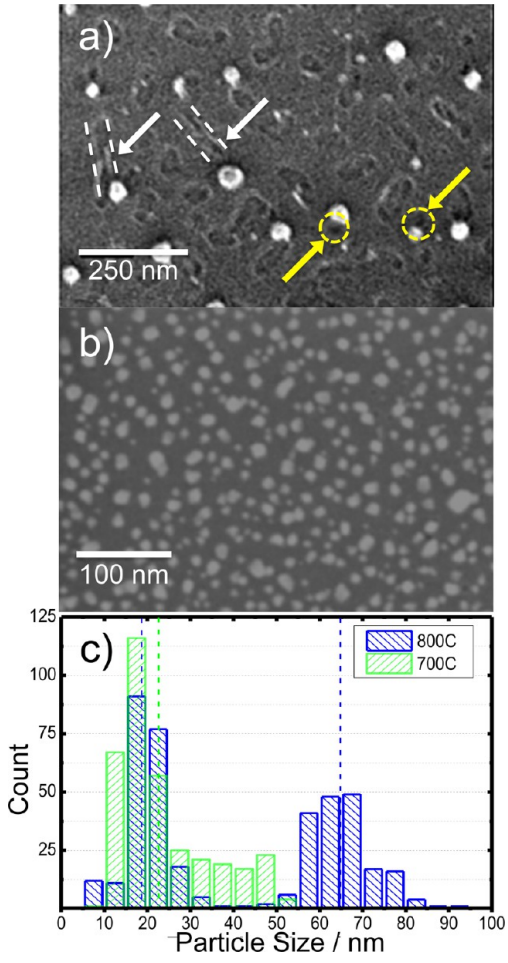

Figure 3. (a, b) SEM images of Ni catalyst nanoparticles on a graphene substrate created via thermal treatment of a Ni thin film at 800 and 700 °C, respectively. The yellow and white arrows and dashed circles and lines in panel a identify etched sites resulting from stationary and mobile nanoparticles, respectively. (c) Histogram of nanoparticle size. The 800 °C growth displays a bimodal shape with two mean diameters at 19.3 ± 5.3 and 64.5 ± 7.9 nm. The 700 °C is unimodal with a mean diameter of 23.2 ± 7.7 nm. The error values are 1 standard deviation from the mean.

We next analyzed the catalyst nanoparticle generation of a 3 nm Ni film atop graphene at 700 °C under Ar/H_2 (400/50 sccm). At this temperature, in contrast with the 800 °C data point, the Ni nanoparticles had higher density on the graphene sheet (Figure 3b) with smaller diameter variation (Figure 3c). Here, the only active hydrogen reaction is hydrogen reduction,[33] which produces high-density nanoparticles with even, circular cross sections (Figure S3). Without the presence of the hydrogenation effect or surface diffusion of the nanoparticles, damage to the graphene sheet was observed to be negligible. It is important to note here that in addition to the benefit of unetched graphene, well-shaped, high-density catalyst nanoparticles lead to vertical, high-density CNTs because of van der Waal attractions, providing more active surface area for the envisioned energy storage applications.[10]

Having established the effect of temperature on the integrity of the graphene substrate during catalyst nanoparticle formation, we then analyzed the impact of CNT growth conditions on graphene etching. In Figure 4a, catalyst nanoparticle generation and CNT growth was accomplished at a reaction temperature of 800 °C. CNTs with a relatively low density (approximately 2.8 × 10^9 cm^{-2}) were grown (Figure 4b). The observation of Ni nanoparticles near the topmost layers strongly suggests top-down growth, confirming the mobility of Ni nanoparticles from the thermal treatment step. The bottom-side of the graphene-CNT sample in Figure 4c (i.e., the side contacting SiO_2) shows a dramatic change in both the morphology of CNTs and the extent of graphene etching during the CNT growth. The graphene layer appears to have been fully etched away; the etched sites formed during catalyst nanoparticle generation are enlarged by hydrogen etching[34] from excess H_2 generated by the decomposition of C_2H_4. Additionally, the diameters of CNTs near the bottom-side are larger (38 ± 13 nm), whereas growth away from the graphene layer produced smaller-diameter CNTs (9.2 ± 1.5 nm). These means were extracted from multiple SEM images. This evidence suggests two stages of the CNT growth; one stage proceeding from both carbon feedstock and graphene as the carbon source via etching and the second stage based solely on the carbon feedstock gas as carbon availability from the graphene diminished and the graphene layer was completely etched.

For comparison, consider Figure 5 wherein catalyst nanoparticles were generated at 700 °C but CNT growth was performed at 800 °C. The mean CNT diameter near the graphene substrate is 25 ± 7 nm. Here, we observed only partial etching of the graphene layer. The Ni nanoparticles are still present near the graphene substrate, and the circular shape of the etched tracks at the point of contact indicate that the

dx.doi.org/10.1021/cm402052z | Chem. Mater. 2013, 25, 3874−3879

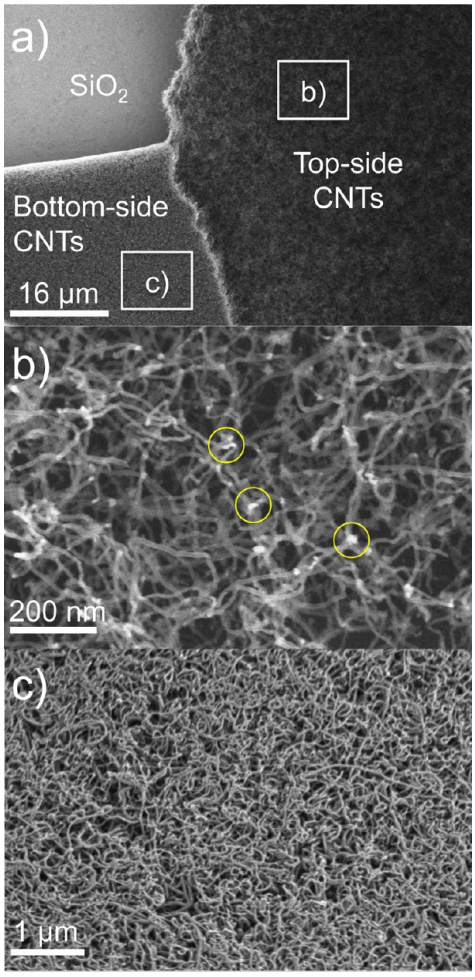

Figure 4. SEM images of CNTs grown on graphene at 800 °C under gas flows of $Ar/H_2/C_2H_4$ = 400/50/50 sccm. Here, Ni catalyst nanoparticles were created at 800 °C. (a) Top view of CNTs as-grown from catalysts on graphene. The sample is intentionally broken and peeled off for the purpose of observation. (b) Magnification of the top-side CNTs. The catalyst nanoparticles are outlined with yellow circles. (c) Magnification of the bottom-side of the graphene-CNT sample with no graphene (fully etched away).

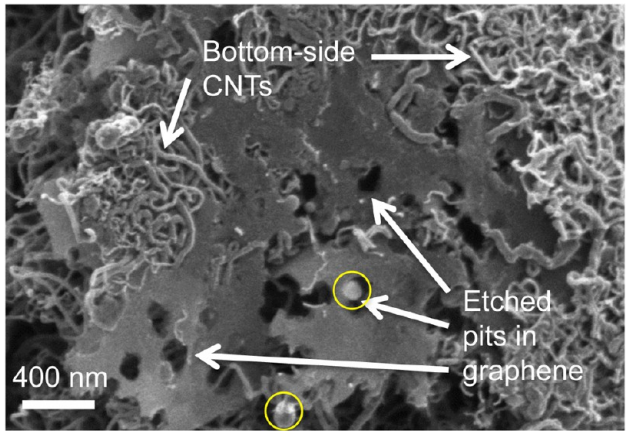

Figure 5. SEM image of the bottom side of a graphene-CNT sample with partially etched graphene grown under gas flows $Ar/H_2/C_2H_4$ = 400/50/50 sccm. Here, Ni catalyst nanoparticles were generated at 700 °C, whereas CNT growth with C_2H_4 occurred at 800 °C. The catalyst nanoparticles are outlined with yellow circles.

particles are largely nonmobile during the growth step and, further, that the additional H_2 from C_2H_4, which specifically decomposes near the catalyst nanoparticle, contributes to the hydrogenation reaction that can only occur at high temperature. We now discuss the difference between the 700 and 800 °C reactions.

The catalytic hydrogenation reaction tends to increase at a high temperature (800 °C) where the density of the catalyst nanoparticles is low[11−13] because the reaction equilibrium between the source hydrocarbon decomposition and carbon saturation into and precipitation from the catalyst nanoparticles shifts toward the consumption of graphene at the nanoparticle−graphene contact interface.[13] In general, as the Ni catalysts become supersaturated with carbon (from thermally decomposed hydrocarbon gas) toward CNT growth, the hydrogenation process limits the supersaturation state by removing carbon on the surface of the catalyst.[11−13] However, in the case of etching, because the Ni catalyst density is low, this carbon removal extends to the graphene layer. Therefore, the graphene layer is etched via hydrogenation in a concentrated hydrogen environment supplied both by an H_2 source and the decomposed hydrocarbon source gases (such as CH_4 or C_2H_4) at high temperature. The catalyst generation process would then yield etched sites in graphene, which would become further enlarged during the CNT growth process, especially at 800 °C.

In clear contrast, Figure 6 shows the successful fabrication of CNTs on graphene at 700 °C. In Figure 6a, a high area density of CNTs with mean diameter of 24 ± 3 nm (Figure 6b) were directly grown on the graphene substrate without prominent signs of graphene etching. Similar CNT diameters were produced in Figure 5b because catalyst generation in both cases was at 700 °C, with a larger standard deviation because some of the carbon source originated from the graphene. The successful result in Figure 6 is attributed to the lower process temperature of 700 °C, which produces highly dense Ni catalyst nanoparticles and curbs etching of the graphene substrate (Figure 6c) during catalyst generation and CNT growth. Such conditions cannot be obtained at 800 °C or higher, temperatures that are necessary to grow CNTs when using CH_4 as the source gas (Figure S4).[16] Therefore, the process conditions selected for CVD growth of CNTs directly on graphene, such as catalyst nanoparticle density and the type of hydrocarbon gas, which impacts the growth temperature and concentration of carbon and hydrogen in the reactor, should be carefully tuned to reduce the incidence of graphene etching by suppressing hydrogenation.

We have studied the graphene-etching phenomena occurring during the direct growth of CNTs on graphene, and we have identified an approach to reduce etching of the graphene substrate by using C_2H_4 gas. We have shown that at high temperatures (800 °C) a catalytic hydrogenation reaction results in the primary growth of etched pits and lines on the graphene layer followed by the expansion of the etched sites via excess hydrogen during the CNT growth process. By using C_2H_4 gas as a hydrocarbon source for CNT growth under low temperature (700 °C) and controlled gas ratio conditions, the catalytic hydrogenation reaction was dramatically suppressed to avoid etching of graphene during the CNT growth process. The successful fabrication of graphene-CNT structures has exceptional implications in applications where the continuity and integrity of the graphene layer is preserved.

dx.doi.org/10.1021/cm402052z | Chem. Mater. 2013, 25, 3874−3879

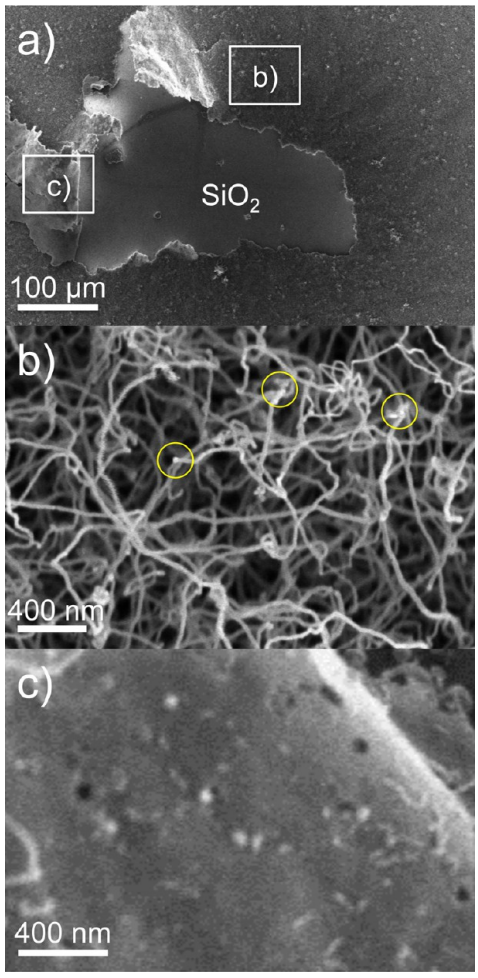

Figure 6. SEM images of CNTs directly grown on graphene at 700 °C under gas flows of $Ar/H_2/C_2H_4$ = 400/50/50 sccm. Here, Ni catalyst nanoparticles were formed at 700 °C. (a) Top view of CNTs as-grown on graphene. The sample is intentionally broken and peeled off for the purpose of observation. (b) Magnification of the top-side CNTs. The catalyst nanoparticles are outlined with yellow circles. (c) Magnification of the bottom side of the graphene-CNT sample with little to no graphene etching. The few CNTs observed in panel c are the result of the mechanical scratching and peeling steps used to prepare the sample for SEM observation and are not related to graphene etching.

EXPERIMENTAL SECTION

Large-area graphene layers were grown on Cu foil (99.99% purity) by atmospheric pressure chemical vapor deposition (APCVD).[10,35] A rolled Cu foil (13 × 60 cm^2) was placed at the center of a 2 in. quartz tube in a horizontal three zone CVD reactor and heated to 1000 °C under a flow of H_2 and Ar. A high-temperature annealing step was carried out to increase the grain size of the Cu foil, ensuring high-quality graphene films. During the growth step, CH_4, H_2, and Ar were fed through the system at flow rates of 50, 15, and 1000 sccm, respectively, for 4 min. Subsequently, the sample was rapidly cooled to room temperature by flowing pressurized H_2 and Ar gases in the furnace. Thermal tape was then attached to the graphene/Cu stack and a force of 9.8 N cm^{-2} was applied to ensure adhesion between the tape and graphene. The Cu foil was fully etched using citric acid Cu etchant (Transene, Inc.) followed by several deionized (DI) water baths to remove the residual etchant. The tape/graphene stack was transferred to a cleaned SiO_2 wafer (4 in.), and uniform force was applied for 10 min. The substrate was heated at 123 °C to detach the thermal tape, and any remaining adhesive residue was removed with boiling acetone (90 °C) and DI water.

After this transfer, approximately 3 nm of the Ni catalyst film was deposited on the graphene layer via electron beam deposition using an Explorer 14 (Denton Vacuum) PVD evaporator. The catalyst/graphene sample was then placed in the CVD reactor and heated to the desired growth temperature while flowing Ar gas in preparation for the introduction of the reaction source gas. The sample was held for 30−45 min at the desired temperature to ensure the thermal breakdown of the Ni thin film into catalyst nanoparticles. After this step, if necessary, the reaction temperature was adjusted, and a mixture of C_2H_4 (99.97%, GTS Welco), H_2, and Ar gases was flown through the furnace for CNT growth on graphene via the vapor−liquid−solid (VLS) process within the Ni catalysts. After the growth was completed, the tube was cooled to room temperature under Ar flow (400 sccm) only.

For TEM imaging, an as-grown graphene-CNT sample was sonicated in ethanol to obtain a low-density, uniform solution of the material. A microdropper was used to drop this solution on a lacey carbon TEM grid. Low-magnification TEM images of likely graphene-CNT areas were taken using an FEI CM20 field-emission S/TEM with 200 kV. After pinpointing such regions, high-magnification TEM images were taken using a JEOL JEM2100F transmission electron microscope at 200 kV.

ASSOCIATED CONTENT

Supporting Information

TEM images of graphene and carbon nanofibers, AFM images of graphene and catalyst nanoparticles, SEM images of CH_4 growth of CNTs, and optical transmission spectra and Raman spectra of graphene and graphene-CNT samples (PDF). This material is available free of charge via the Internet at http://pubs.acs.org.

AUTHOR INFORMATION

Corresponding Author

*E-mail: eyang@stevens.edu.

Author Contributions

The manuscript was written through contributions of all authors. All authors have given approval to the final version of the manuscript.

Funding

This work was supported by the Robert Crooks Stanley Fellowship, the National Science Foundation (DMR-0922522, EECS-1040007, ECCS-1104870, and EEC-1138244), and the Air Force Office for Scientific Research (FA9550-11-1-0272 and FA9550-12-1-0326).

Notes

The authors declare no competing financial interest.

REFERENCES

(1) Young Kim, J.; Jang, J.-W.; Hyun Youn, D.; Yul Kim, J.; Sun Kim, E.; Sung Lee, J. *RSC Adv.* **2012**, *2*, 9415−9422.
(2) Li, C.; Li, Z.; Zhu, H.; Wang, K.; Wei, J.; Li, X.; Sun, P.; Zhang, H.; Wu, D. *J. Phys. Chem. C* **2010**, *114*, 14008−14012.
(3) Tai, Z.; Yan, X.; Lang, J.; Xue, Q. *J. Power Sources* **2012**, *199*, 373−378.
(4) Wu, Q.; Xu, Y. X.; Yao, Z. Y.; Liu, A. R.; Shi, G. Q. *ACS Nano* **2010**, *4*, 1963−1970.
(5) Dai, G.-P.; Wu, M. H.; Taylor, D. K.; Brennaman, M. K.; Vinodgopal, K. *RSC Adv.* **2012**, *2*, 8965−8968.
(6) Fan, Z.-J.; Yan, J.; Wei, T.; Ning, G.-Q.; Zhi, L.-J.; Liu, J.-C.; Cao, D.-X.; Wang, G.-L.; Wei, F. *ACS Nano* **2013**, *5*, 2787−2794.
(7) Kim, U. J.; Lee, I. H.; Bae, J. J.; Lee, S.; Han, G. H.; Chae, S. J.; Gunes, F.; Choi, J. H.; Baik, C. W.; Kim, S. I.; Kim, J. M.; Lee, Y. H. *Adv. Mater.* **2011**, *23*, 3808−3808.
(8) Paul, R. K.; Ghazinejad, M.; Penchev, M.; Lin, J.; Ozkan, M.; Ozkan, C. S. *Small* **2010**, *6*, 2309−2313.

(9) Rao, R.; Chen, G.; Arava, L. M. R.; Kalaga, K.; Ishigami, M.; Heinz, T. F.; Ajayan, P. M.; Harutyunyan, A. R. *Sci. Rep.* **2013**, *3*, 1891-1−1891-6.
(10) Kim, Y.-S.; Kumar, K.; Fisher, F. T.; Yang, E.-H. *Nanotechnology* **2011**, *23*, 015301.
(11) Hunley, D. P.; Johnson, S. L.; Stieha, J. K.; Sundararajan, A.; Meacham, A. T.; Ivanov, I. N.; Strachan, D. R. *ACS Nano* **2011**, *5*, 6403−6409.
(12) Campos, L. C.; Manfrinato, V. R.; Sanchez-Yamagishi, J. D.; Kong, J.; Jarillo-Herrero, P. *Nano Lett.* **2009**, *9*, 2600−2604.
(13) Biró, L. P.; Lambin, P. *Carbon* **2010**, *48*, 2677−2689.
(14) Schäffel, F.; Warner, J. H.; Bachmatiuk, A.; Rellinghaus, B.; Büchner, B.; Schultz, L.; Rümmeli, M. H. *Nano Res.* **2009**, *2*, 695−705.
(15) Tran, P. A.; Zhang, L.; Webster, T. J. *Adv. Drug Delivery Rev.* **2009**, *61*, 1097−1114.
(16) Son, S. Y.; Lee, Y.; Won, S.; Lee, D. H.; Kim, S. D.; Sung, S. W. *Ind. Eng. Chem. Res.* **2008**, *47*, 2166−2175.
(17) Kumar, K.; Kim, Y. S.; Yang, E. H. *Carbon* **2013**, in press.
(18) Zhu, Y.; Li, L.; Zhang, C.; Casillas, G.; Sun, Z.; Yan, Z.; Ruan, G.; Peng, Z.; Raji, A.-R. O.; Kittrell, C.; Hauge, R. H.; Tour, J. M. *Nat. Commun.* **2012**, *3*, 1225-1−1225-7.
(19) Novaes, F. D.; Rurali, R.; Ordejón, P. *ACS Nano* **2010**, *4*, 7596−7602.
(20) Ferrari, A. C.; Basko, D. M. *Nat. Nanotechnol.* **2013**, *8*, 235−246.
(21) Bissett, M. A.; Izumida, W.; Saito, R.; Ago, H. *ACS Nano* **2012**, *6*, 10229−10238.
(22) Ferrari, A. C.; Meyer, J. C.; Scardaci, V.; Casiraghi, C.; Lazzeri, M.; Mauri, F.; Piscanec, S.; Jiang, D.; Novoselov, K. S.; Roth, S.; Geim, A. K. *Phys. Rev. Lett.* **2006**, *97*, 187401-1−187401-4.
(23) Costa, S.; Borowiak-Palen, E.; Kruszynska, M.; Bachmatiuk, A.; Kalenczuk, R. J. *Mater. Sci.—Pol.* **2008**, *26*, 433−441.
(24) Zdrojek, M.; Gebicki, W.; Jastrzebsi, C.; Melin, T.; Huczko, A. *Solid State Phenom.* **2004**, *99−100*, 265−268.
(25) Benoit, J.; Buisson, J.; Chauvet, O.; Godon, C.; Lefrant, S. *Phys. Rev. B* **2002**, *66*, 073417-1−073417-4.
(26) Giermann, A. L.; Thompson, C. V. *Appl. Phys. Lett.* **2005**, *86*, 121903-1−121903-3.
(27) Kondic, L.; Diez, J.; Rack, P.; Guan, Y.; Fowlkes, J. *Phys. Rev. E* **2009**, *79*, 026302-1−026302-7.
(28) Randolph, S. J.; Fowlkes, J. D.; Melechko, A. V.; Klein, K. L.; Meyer, H. M.; Simpson, M. L.; Rack, P. D. *Nanotechnology* **2007**, *18*, 465304.
(29) Tomita, A.; Tamai, Y. *J. Phys. Chem.* **1974**, *78*, 2254−2258.
(30) Carey, J. D.; Ong, L. L.; Silva, S. R. P. *Nanotechnology* **2003**, *14*, 1223−1227.
(31) Klinke, C.; Bonard, J.-M.; Kern, K. *J. Phys. Chem. B* **2004**, *108*, 11357−11360.
(32) Hennig, G. R. *J. Inorg. Nucl. Chem.* **1962**, *24*, 1129−1132.
(33) Geissler, A.; He, M.; Benoit, J.-M.; Petit, P. *J. Phys. Chem. C* **2010**, *114*, 89−92.
(34) Zhang, Y.; Li, Z.; Kim, P.; Zhang, L.; Zhou, C. *ACS Nano* **2012**, *6*, 126−132.
(35) Bae, S.; Kim, H.; Lee, Y.; Xu, X.; Park, J.-S.; Zheng, Y.; Balakrishnan, J.; Lei, T.; Kim, H. R.; Song, I. Y.; Kim, Y.-J.; Kim, K. S.; Özyilmaz, B.; Ahn, J.-H.; Hong, B. H.; Iijima, S. *Nat. Nanotechnol.* **2010**, *5*, 574−578.